Composites Part B 134 (2018) 18–27

Contents lists available at ScienceDirect

Composites Part B

journal homepage: www.elsevier.com/locate/compositesb

Capacitance-based nondestructive detection of aggregate proportion variation in a cement-based slab

Yulin Wang [1], D.D.L. Chung*

Composite Materials Research Laboratory, Department of Mechanical and Aerospace Engineering, University at Buffalo, The State University of New York, Buffalo, NY 14260–4400, USA

ARTICLE INFO

Article history:
Received 12 June 2017
Received in revised form
5 September 2017
Accepted 7 September 2017
Available online 22 September 2017

Keywords:
Ceramic-matrix composites (CMCs)
Particle-reinforcement
Electrical properties
Non-destructive testing
Capacitance

ABSTRACT

This paper reports unprecedentedly capacitance-based nondestructive detection of aggregate proportion variation in cement-based materials. It uses the fringing electric field of a capacitor comprising a cement-based slab and two relatively small copper electrodes. The aggregate volume fraction increases from cement paste to mortar and to concrete, thus causing the apparent permittivity (high due to the fringing field) to decrease in the same order. Each slab consists of two regions with different aggregate proportions. The through-thickness and in-plane capacitances are measured using sandwiching and coplanar electrodes, respectively. To locate the interface, the capacitance is innovatively measured using a series of electrodes.

1. Introduction

Aggregates are important in cement-based materials as reinforcement and drying shrinkage restrainer. Thus, the spatial variation in the aggregate proportion in a cement-based structure can result in undesirable spatial variation in the mechanical properties and drying shrinkage. In a cured cement-based material, a higher aggregate proportion corresponds to a lower cement paste proportion. Since the cement paste is the binder for the aggregates, its amount must be adequate.

Aggregate proportion variation can occur due to the separate pouring of the cement-based mix in different sections of a large structure. It can also occur due to the variation in aggregate size. Furthermore, it can occur in the repair of a concrete structure using new concrete that differs in mix design from the old concrete present in the structure.

Aggregate proportion variation does not necessarily result in defects (such as voids and cracks) at the interface between parts that involve different aggregate proportions. Thus, techniques (such as ultrasonic inspection) that focus on the detection of defects are not adequate for the detection of aggregate proportion variation. Moreover, aggregate proportion variation does not necessarily result in significant variation in the radio wave reflection/absorption behavior, so techniques involving radars are not adequate for the detection of aggregate proportion variation.

The true permittivity of cement-based materials does not vary over a wide range upon loading [1] or upon admixture addition [2], so the true permittivity is not sufficiently sensitive to the aggregate proportion or defects. However, we recently reported that, when the capacitance is unconventionally measured using electrodes (electrical contacts) that are smaller in area than the cement-based material being sandwiched by the electrodes, the fringing electric field is substantial and greatly increases the apparent (measured) relative permittivity of the cement-based material [3].

The apparent relative permittivity (2 kHz) increases with increasing thickness, due to the increasing fringing field with increasing thickness. For plain cement paste of various thicknesses, it ranges from 150 to 375. In contrast, when the electrodes conventionally cover the entire area of the cement-based material, the fringing field effect is much weaker, so that the apparent relative permittivity is much lower, ranging from 24 to 38 for plain cement paste of various thicknesses.

As a consequence of the high apparent permittivity, the fringing

* Corresponding author.
E-mail address: ddlchung@buffalo.edu (D.D.L. Chung).
URL: http://alum.mit.edu/www/ddlchung
[1] Permanent address: College of Civil Engineering and Architecture, Wuyi University, Wuyi Road 16, Xinfeng street, Wuyi Shan City, Fujian Province 354300, China.

https://doi.org/10.1016/j.compositesb.2017.09.015
1359-8368/

field allows the apparent permittivity and the associated capacitance to provide nondestructive detection of defects in a cement-based material [4]. In this paper, we investigate for the first time the use of this technique to detect a microstructural aspect that is more subtle than defects, namely the aggregate proportion variation in a cement-based slab.

The total aggregate proportion inversely relates to the proportion that is not in the form of aggregates, i.e., the proportion that is cement paste. The technique of this work is based on the detection of the proportion that is cement paste rather than detecting directly the proportion that is in the form of aggregates.

This work is not directed at detecting the aggregate or cement paste proportion, but is directed at detecting the variation in the proportion. In particular, this work concerns the determination of the location of the interface between regions that differ in the aggregate proportion. For the sake of demonstrating the feasibility of the concept, this work uses aggregate proportions that correspond to those of cement paste, mortar and concrete. The determination of the minimum detectable aggregate variation is beyond the scope of this work. Furthermore, the variation used in this work for the sake of feasibility demonstration is associated with the presence of contiguous regions in the same slab, such that the regions differ in the aggregate proportion.

The objectives of this work are (i) to demonstrate the feasibility of using capacitance measurement to detect aggregate proportion variation (i.e., cement paste proportion variation) in a cement-based slab, (ii) to provide a methodology for capacitance-based detection of aggregate proportion variation in a cement-based slab, and (iii) to investigate the effects of aggregate proportions on the apparent permittivity and capacitance of a cement-based material.

2. Methods

2.1. Materials

Portland cement (Type I, ASTM C150, from Lafarge Corp., Southfield, MI) is used. The density of the cement powder is 3.15 ± 0.02 g/cm^3 (measured in this work and the same as the previously reported value of 3.15 g/cm^3 [5,6]). The cement-based materials studied are cement paste, mortar and concrete. The water/cement ratio is 0.35, 0.55 and 0.42 for cement paste, mortar and concrete, respectively. The fine aggregate is sand with true density 2.55 g/cm^3 (measured in this work). The sand/cement mass ratio in the mortar is 3.0. The coarse aggregate is gravel with true density 2.59 g/cm^3 (measured in this work). The mass ratio of cement to fine aggregate to coarse aggregate in the concrete is 1: 1.3: 2.2.

Silica fume (Elkem Materials Inc., Pittsburgh, PA, microsilica, EMS 965, USA) is used at 15% by mass of cement, as in prior work [7]; it has particle size ranging from 0.03 to 0.5 μm, with average size 0.2 μm; its true density is 2.2 g/cm^3; it contains >93 wt% SiO_2, <0.7 wt% Al_2O_3, <0.7 wt% CaO, <0.7 wt% MgO, <0.5 wt% Fe_2O_3, <0.4 wt% Na_2O, <0.9 wt% K_2O, and <6 wt% loss on ignition. The silica fume has been subjected to silane treatment in order to improve its dispersion in the cement mix [8,9]. The silane coupling agent is a 1:1 (by mass) mixture of Z-6020 ($H_2NCH_2CH_2NHCH_2CH_2CH_2Si(OCH_3)_3$) and Z-6040 ($OCH_2$-$CHCH_2OCH_2CH_2CH_2Si(OCH_3)_3$) from Dow Corning Corp. (Midland, MI). The amine group in Z-6020 serves as a catalyst for the curing of the epoxy and consequently allows the Z-6020 molecule to attach to the epoxy end of the Z-6040 molecule. The trimethylsiloxy ends of the Z-6020 and Z-6040 molecules then connect to the −OH functional group on the surface of the silica fume. The silane is dissolved in ethylacetate to form a solution with 2.0 wt% silane. Surface treatment of the silica fume is performed by immersion in the silane solution, heating to 75 °C while stirring, and then holding at 75 °C for 1.0 h, followed by filtration and drying. Subsequently, the silica fume is heated at 110 °C for 12 h [8,9].

The silane treatment increases the density of the 28-day cured silica-fume cement paste from 1.72 to 1.73 g/cm^3 [10]. Hence, the effect of the silane treatment on the density is small.

A high-range water reducing agent (Glenium 3000NS, BASF Construction Chemicals) is used at 1.0% by mass of cement. The defoamer (Colloids Inc., Marietta, GA, 1010, USA) is used at 0.13% (% of specimen volume).

Cement powder and silica fume are dry mixed by using a rotary mixer with a flat beater without water addition for about 3 min. Then water is gradually added to the mixture while mixing continues for an additional period of 5 min. After this, the fine aggregate is added in case of the preparation of mortar, whereas both fine and coarse aggregates are added in case of the preparation of concrete.

The cement-based material specimens are in the form of rectangular slabs of size 300 mm × 150 mm x 19.5 mm. Cement-based mixes with different aggregate proportions are poured to the two halves of the oiled plastic mold, using a thin cardboard partition to separate the two halves during pouring. The size of each half is 150 × 150 mm (Fig. 1). For all specimens, after filling the mold, an external vibrator is used to facilitate compaction and diminish the air bubbles. The specimens are demolded after 24 h and then cured at a relative humidity of nearly 100% for 28 days. The demolded specimens are ground and burnished to ensure that the surfaces are smooth before capacitance measurement.

2.2. Methodology

2.2.1. Permittivity measurement

The measurement of the relative permittivity typically involves a parallel-plate capacitor configuration, with the specimen under investigation being sandwiched by electrodes [2]. There is an electrically insulating plastic film positioned between the specimen and each electrode, as necessitated by the fact that the RLC meter used for the capacitance measurement, as typical for RLC meters, is not designed for measuring the capacitance of a conductive material. Although cement in the absence of a conductive admixture is only slightly conductive, the use of an insulating (dielectric) film is recommended and is used in this work. The electrodes are in the form of copper foils. The electrode, plastic sheet and cement-based specimen in the form of a stack are held together by adhesion.

The relative permittivity κ in the direction perpendicular to the plane of the sandwich is given by the equation

$$C_v = \varepsilon_o \kappa A_s/l, \quad (1)$$

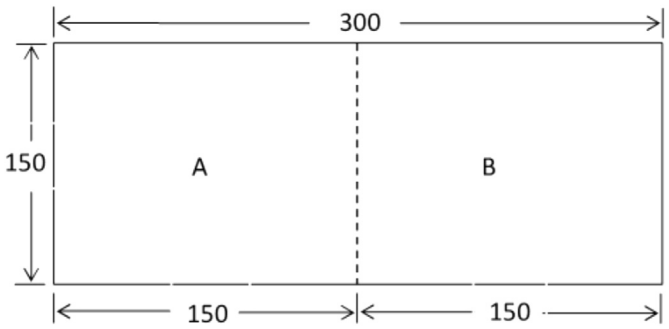

Fig. 1. Specimen configuration. A single rectangular specimen (300 mm × 150 mm) consists of two regions (A and B) of equal size (each 150 mm × 150 mm) but different aggregate proportions. All dimensions are in mm.

where C_v is the capacitance due to the volume of the specimen, ε_o is the permittivity of free space (8.85×10^{-12} F/m), A_s is the area of the sandwich (i.e., the area of the electrode), and l is the thickness of the specimen sandwiched by the electrodes.

The fringing electric field refers to the electric field in the surrounding medium immediately beyond the rim of the parallel-plate capacitor geometry. The fringing field results in the measured capacitance to be higher than the expected value. This is because the fringing electric field causes the specimen area to be effectively larger than the true area. As a consequence, the measured (apparent) permittivity is higher than the true value. The higher is the permittivity of the surrounding medium, the greater is the fringing field effect and the higher is the apparent permittivity. In this work, the surrounding medium is the cement-based material being evaluated, as provided by the use of electrodes that are smaller in area than the cement-based material [3]. In other words, the cement-based material extends beyond the electrodes.

2.2.2. Decoupling the volumetric and interfacial contributions to the measured capacitance

The interface between the specimen and the electrode (whether there is an insulating film at the interface or not) affects the measured capacitance. A method of decoupling the volumetric and interfacial contributions to the measured capacitance involves testing multiple electrode-specimen-electrode sandwiches with different areas, but the same thickness [3]. This is illustrated in Fig. 2 for three areas that are equal to the areas of 1, 2 and 3 squares that are in contact and lined up along an edge of the square in the same plane and the same direction. The measured capacitance C_m is given by the equation for capacitances in parallel, i.e.,

$$C_m = C_o + \varepsilon_o \kappa NA/l, \quad (2)$$

where N is the number of squares that constitute the electrode and C_o is the capacitance at $N = 0$. The C_o relates to the fringing field effect, as obtained by extrapolating the plot of C_m vs. NA to $N = 0$ (Fig. 3). This method of permittivity measurement is as previously reported and shown to be reliable [3]. Based on Eq. (2), the slope of the plot of C_m vs. NA is equal to $\varepsilon_o \kappa/l$. Thus, κ is obtained from the slope. Since the electrode-specimen interface is structurally identical for all values of NA, the slope effectively removes the interfacial contribution. In case that the electrodes are smaller than the cement-based specimen, the fringing field effect is large and the κ obtained from the slope is the apparent permittivity rather than the true permittivity.

2.2.3. Spatially resolved capacitance measurement

By positioning the electrodes at different points of the cement-based specimen, spatially resolved capacitance measurement is achieved. The capacitance is measured in either the through-thickness direction (configuration A, Fig. 4) or the in-plane direction (configuration B, Fig. 5). The electrodes are either square (for $N = 1$) or rectangular (for $N > 1$), with width equal to 25.0 mm and length equal to the combined length of N squares (Fig. 2).

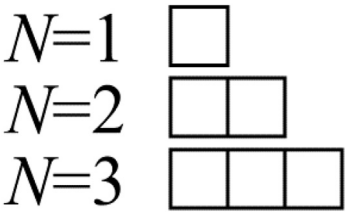

Fig. 2. Illustration of the electrode geometry. The electrode is square for $N = 1$ and is rectangular for $N = 2$ onward. A rectangular electrode has a geometry corresponding to a number of squares that are lined up. The integer N refers to the number of square lined up. The area of each square is A.

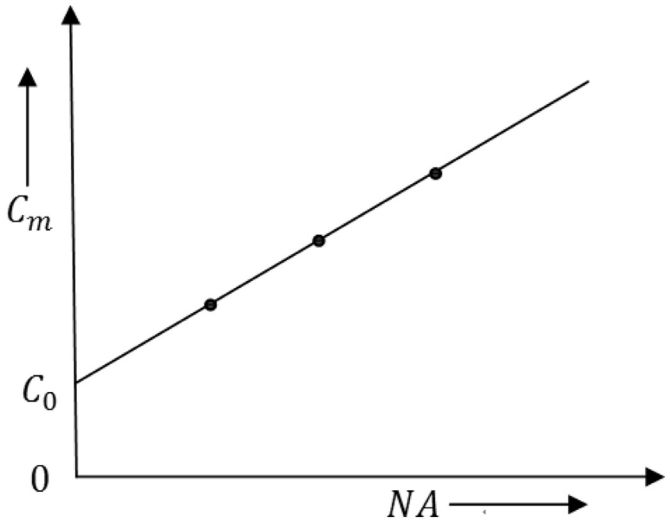

Fig. 3. Schematic plot of C_m vs. the area NA, where N is the number of squares that make up an electrode (Fig. 2) and A is the area of each square in the electrode geometry.

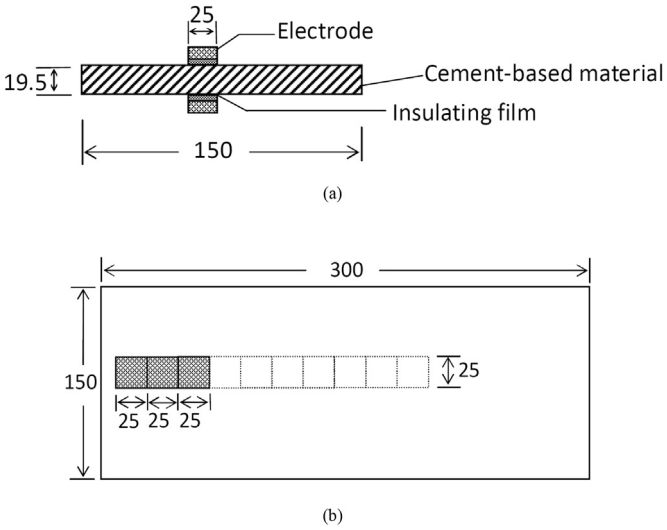

Fig. 4. Configuration A, using two electrodes (each with area = 25 N mm x 25 mm, where N = 1, 2, 3, …, Fig. 2) at the same location on the opposite surfaces of the slab (300 × 150 × 19.5 mm). An electrically insulating (dielectric) film is positioned between the cement-based specimen and the entire area of each electrode. All dimensions are in mm. (a) Side view, showing the 25-mm edge of one of the two locations of the electrode. (b) Top view, showing a series of electrodes for N = 1, 2, 3, ….

In configuration A, the electrodes are directly on top of one another and sandwich the specimen, which extend beyond the electrodes. Configuration A allows determination of the apparent permittivity, because the cross-sectional area of the current path is well defined (except for the fringing field increasing this area beyond the electrode area). In configuration B, the electrodes are coplanar on the same surface of the specimen, such that the proximate edges of the two electrodes are at a distance g apart, with g = 15, 30 or 70 mm. Configuration B does not allow

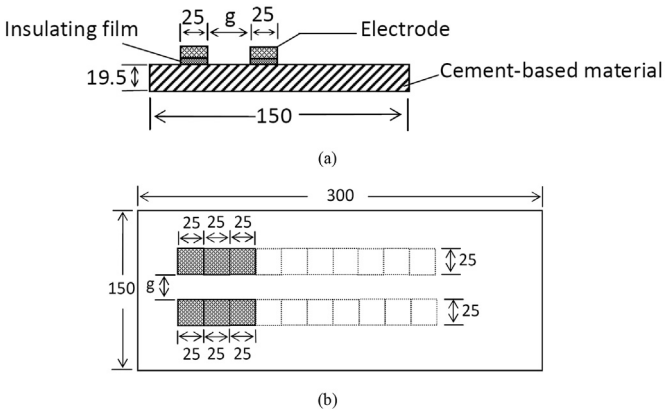

Fig. 5. Configuration B, using two coplanar electrodes (area = 25 *N* mm x 25 mm, where $N = 1, 2, 3, \ldots$, Fig. 2) on the same surface of the slab (300 × 150 × 19.5 mm), with the proximate edges of the two parallel electrodes separated by a distance *g*. An electrically insulating (dielectric) film is positioned between the cement-based specimen and the entire area of each electrode. All dimensions are in mm. (a) Side view, showing the 25-mm edge of each of the two parallel electrodes. (b) Top view, showing in solid lines a series of three pairs of electrode for $N = 1, 2$ and 3. The two electrodes in each pair have the same value of *N* and their proximate edges are separated by a distance *g*.

determination of the apparent permittivity, because the current spreads between the two coplanar electrodes. The spreading causes the cross-sectional area of the current path to be poorly defined. Nevertheless, configuration B is more convenient than configuration A for application to structures, which may not be conveniently accessed from both top and bottom surfaces.

2.2.4. Determination of the interface between regions with different aggregate proportions

In both configurations A and B (Figs. 4 and 5), *N* ranges from 1 to 12 and capacitance measurement is progressively conducted in order of increasing *N*. The interface between regions with different aggregate proportions is between the 6th and 7th squares (Fig. 6). Then the measured capacitance C_m is plotted against *NA*, where *A* is the area of each square. The slope of this linear plot (Fig. 3) differs between the two regions, due to the dependence of the apparent permittivity on the aggregate proportion. The data points corresponding to $N = 1, 2, \ldots,6$ are used to obtain the linear curve for the left region, whereas those corresponding to $N = 7, \ldots, 12$ are used to obtain the linear curve for the right region. In other words, there is a change in slope at the interface between the two regions. By using a series of electrodes that are oriented perpendicular to the interface of the two regions, the location of this interface is determined. In using each series of electrodes, *N* is progressively increased from 1 to 12.

2.2.5. Instrumentation

The capacitance is measured using a precision RLC meter (Instek LCR-816 High Precision LCR Meter, 100 Hz-2 kHz) For configuration A, the through-thickness electric field is 0.013 V/cm. For configuration B, the in-plane electric field corresponds to that of a fixed voltage of 0.25 V between the two coplanar electrodes across the distance *g*, which is varied. The frequency is 2 kHz, though the concept of this work is not restricted to this particular frequency. The measured capacitance is that for the equivalent circuit model in which the capacitance and resistance are in parallel.

2.2.6. Difference from impedance spectroscopy

This work uses a technique that differs greatly from the widely used technique of impedance spectroscopy, which measures the

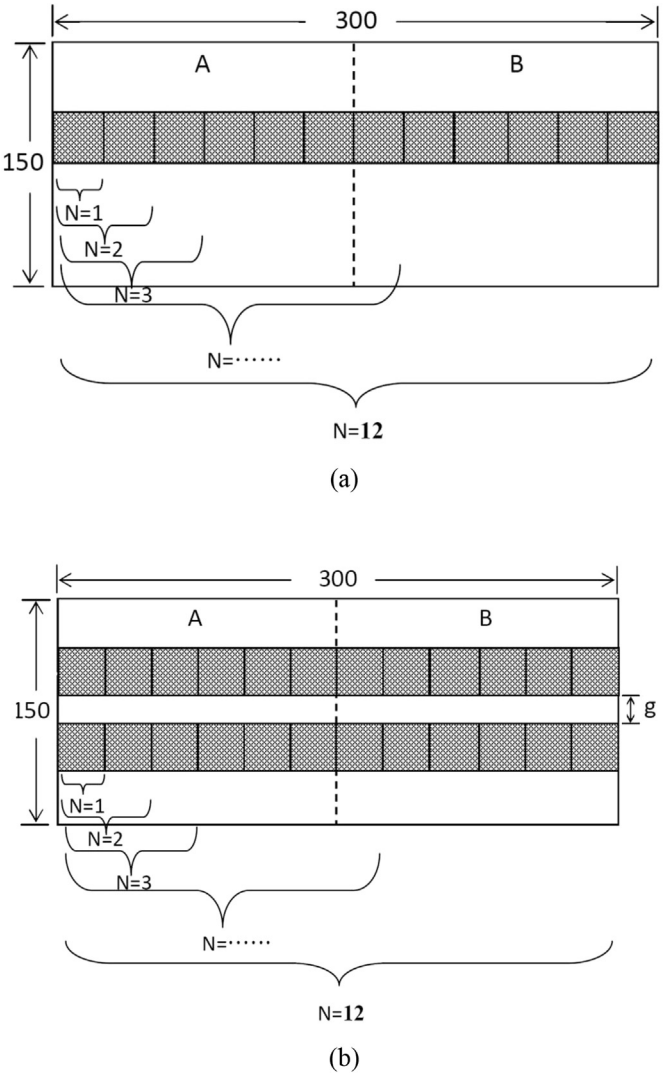

Fig. 6. Top view of the electrode configuration, showing a series of electrodes for $N = 1, 2, \ldots, 12$. The series of electrodes is perpendicular to the interface (dashed line in the middle of the slab) between the two regions and covers both regions. By using a series of electrodes that includes electrodes that extend across the interface of the two regions and that cover parts of both regions, the location of this interface is determined. All dimensions are in mm. (a) Configuration A. (b) Configuration B, with the two parallel electrodes in each pair having the same value of *N* and having their proximate edges separated by distance *g*.

impedance as a function of frequency and uses the frequency dependence to obtain information on the material system. Firstly, the technique of this work does not measure the impedance, but measures the relative permittivity (real part of the permittivity). Secondly, the technique of this work decouples the contribution of the electrode-specimen interface from the contribution of the volume of the specimen. This decoupling is not performed in impedance spectroscopy. Thirdly, the technique of this work does not need to address the frequency dependence in order to obtain meaningful information. In contrast, impedance spectroscopy is focused on the frequency dependence of the impedance, as conventionally described in terms of the Nyquist plot, for the purpose of deriving, by mathematical fitting of the plot, an equivalent electrical circuit that is intended to describe the electrical/dielectric behavior of the material. The circuit model obtained by the curve fitting tends to be not unique, so the determined values of the circuit elements in the model are not very meaningful.

3. Experimental confirmation of methodology

Concerning configuration A, Figs. 7–9 and Table 1 show that the plot of the measured capacitance vs. electrode area is indeed linear in each region, whether the measurement is conducted with increasing *N* in the direction approaching the interface between the two regions or the direction away from this interface. Moreover, the linearity occurs regardless of whether the two regions in contact are (i) paste and mortar, (ii) paste and concrete, or (iii) mortar and concrete. The slope of the curve, which relates to the apparent relative permittivity, is greatest for cement paste, lower for mortar and lowest for concrete, regardless of the direction of the measurement (Table 1). Water is a significant contributor to the permittivity, since the true relative permittivity of water is high (about 80 [11]). The observed decrease of the apparent relative permittivity from paste to mortar and to concrete is consistent with the decreasing volume fraction of paste from paste to mortar and to concrete (Sec. 5) and the fact that the paste, which contains water and cement, contributes much more to the permittivity than the fine or coarse aggregate. Furthermore, the adsorption of water by the aggregate surface reduces the amount of water available for the paste part of the cement-based material, thereby contributing to causing the difference in content and nature of water among concrete, mortar and cement paste. The permittivity of water may differ between the adsorbed water, free water and water in the cured cement paste, but this point is beyond the scope of this work. The apparent relative permittivity values of the cement-based materials are all much higher than the true values, due to the fringing field effect, as previously reported by the same authors [3].

Concerning configuration B, Figs. 10–12 and Table 2 show that

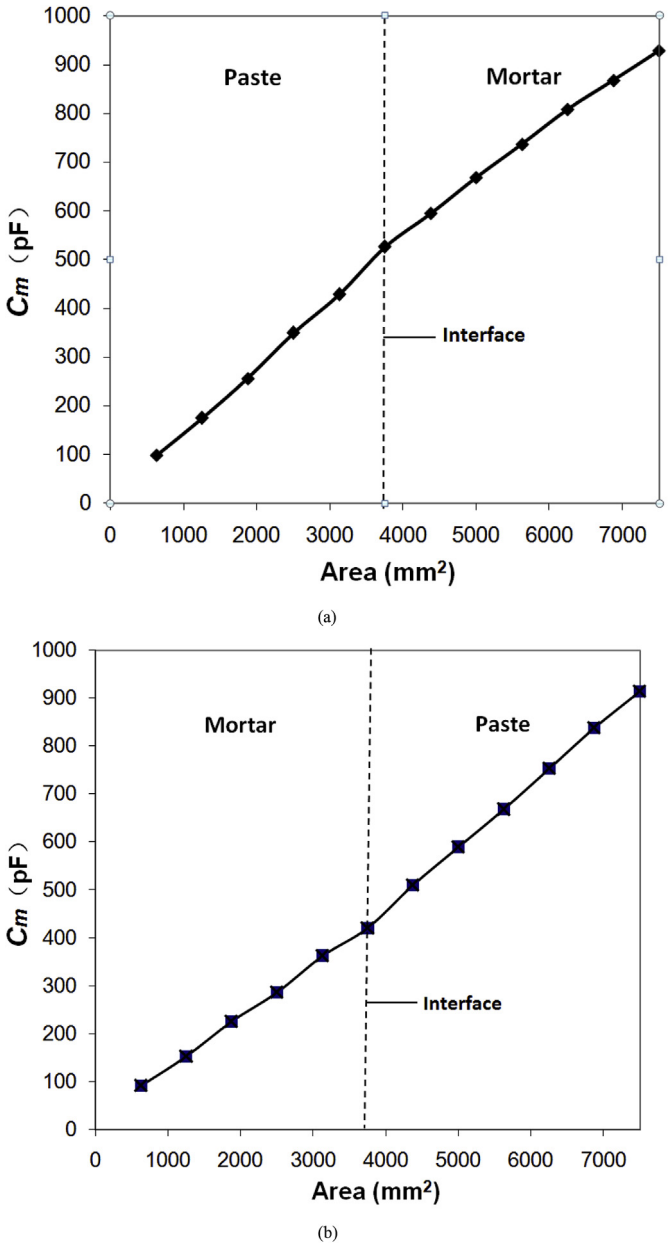

Fig. 7. The plot of the measured capacitance C_m vs. electrode area (*NA*) corresponding to $N = 1, 2, \ldots, 12$ and involving configuration A. The vertical dashed line indicates the location of the interface between the two regions, which are cement paste and mortar. (a) The increase in *N* is in the direction from cement paste to mortar. (b) The increase in *N* is in the direction from mortar to cement paste.

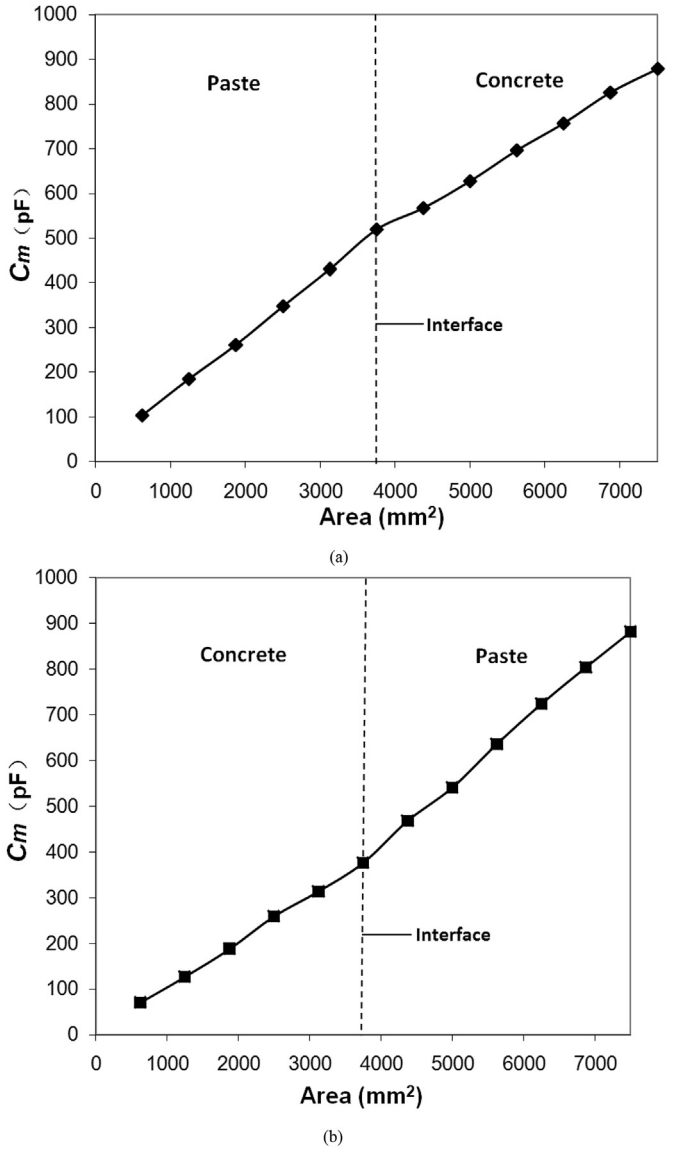

Fig. 8. The plot of the measured capacitance C_m vs. electrode area (*NA*) corresponding to $N = 1, 2, \ldots, 12$ and involving configuration A. The vertical dashed line indicates the location of the interface between the two regions, which are cement paste and concrete. (a) The increase in *N* is in the direction from cement paste to concrete. (b) The increase in *N* is in the direction from concrete to cement paste.

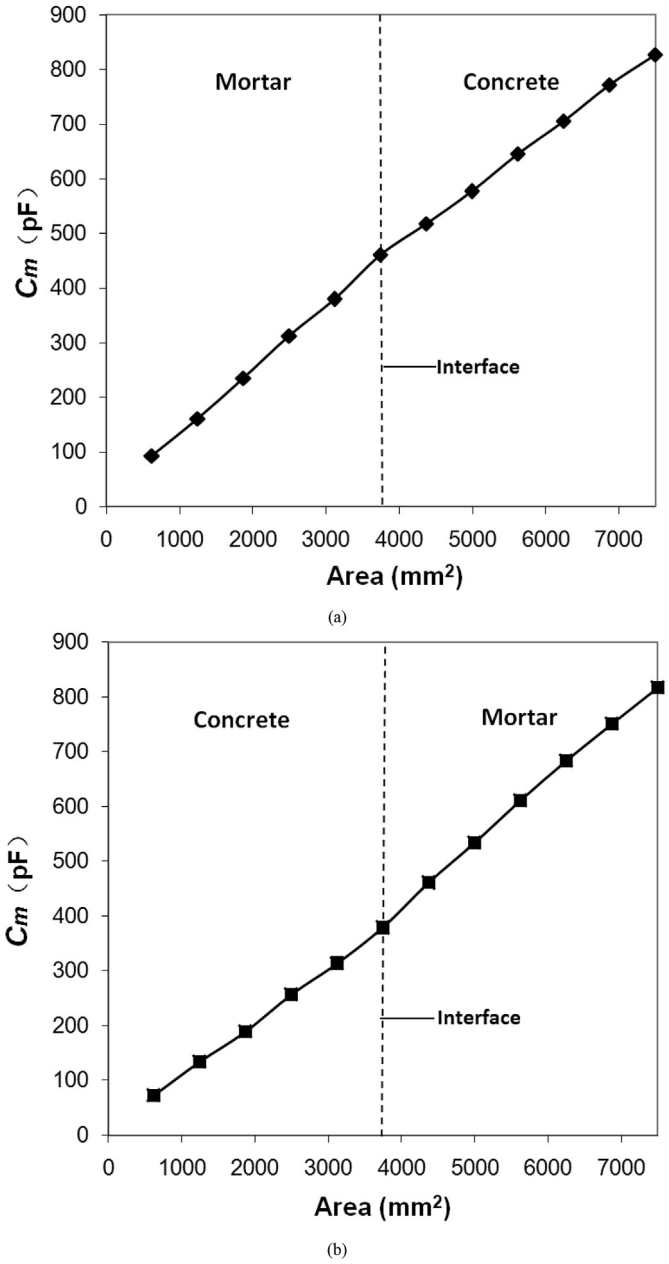

Fig. 9. The plot of the measured capacitance C_m vs. electrode area (NA) corresponding to $N = 1, 2, \ldots, 12$ and involving configuration A. The vertical dashed line indicates the location of the interface between the two regions, which are mortar and concrete. (a) The increase in N is in the direction from mortar to concrete. (b) The increase in N is in the direction from concrete to mortar.

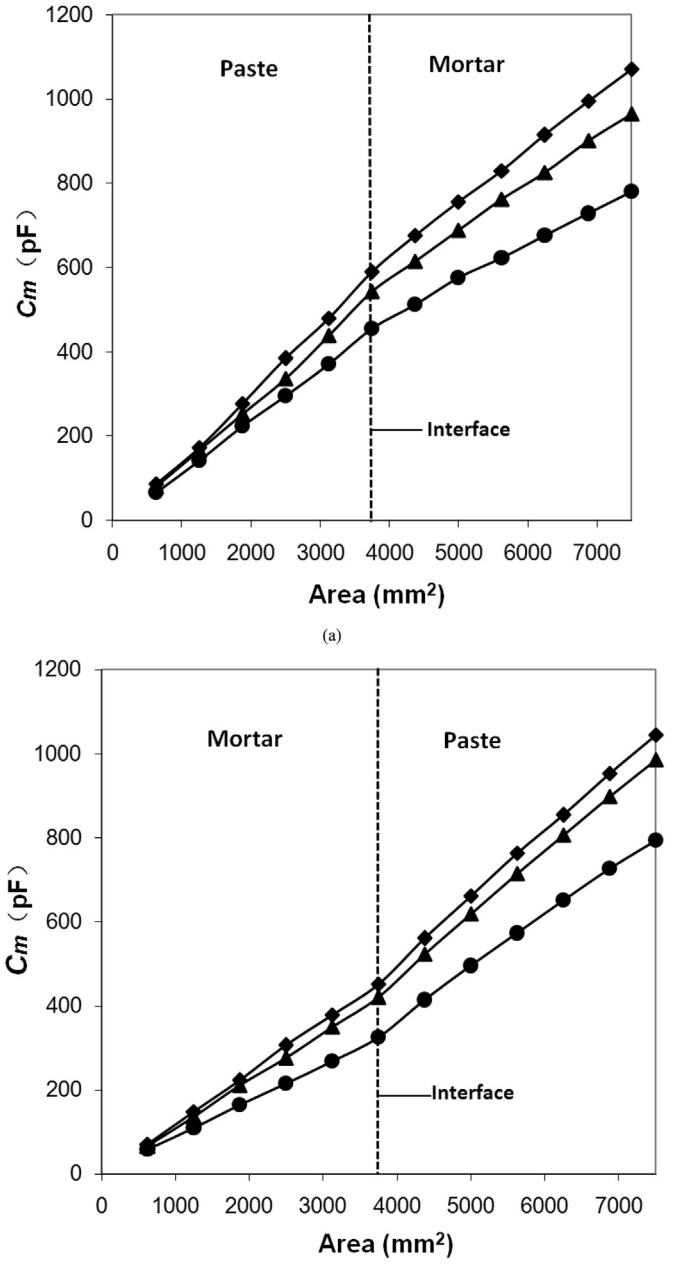

Fig. 10. The plot of the measured capacitance C_m vs. electrode area (NA) corresponding to $N = 1, 2, \ldots, 12$ and involving configuration B. The vertical dashed line indicates the location of the interface between the two regions, which are cement paste and mortar. ◆ $g = 15$ mm, ▲ $g = 30$ mm, ● $g = 70$ mm. (a) The increase in N is in the direction from cement paste to mortar. (b) The increase in N is in the direction from mortar to cement paste.

Table 1
Apparent relative permittivity obtained using configuration A.

Direction of increasing N	Apparent relative permittivity		
	Cement paste	Mortar	Concrete
From paste to mortar	318 ± 33	235 ± 22	/
From mortar to paste	303 ± 31	230 ± 13	/
From mortar to concrete	/	235 ± 19	200 ± 19
From concrete to mortar	/	234 ± 17	200 ± 20
From paste to concrete	307 ± 19	/	208 ± 11
From concrete to paste	311 ± 22	/	210 ± 22

the curve of the measured capacitance vs. the electrode area is indeed linear in each region, regardless of the direction of the measurement with respect to the interface between the two regions, and regardless of whether the two regions in contact are (i) paste and mortar, (ii) paste and concrete, or (iii) mortar and concrete. The slope of the curve is highest for cement paste, lower for mortar, and lowest for concrete. This is consistent with the same trend for the apparent relative permittivity obtained using configuration A. For any region, the greater is g, the smaller is the measured capacitance. This is expected, since g is related to the thickness (distance between the electrodes) of the in-plane capacitor. Thus, for higher sensitivity of the NDE, the use of a

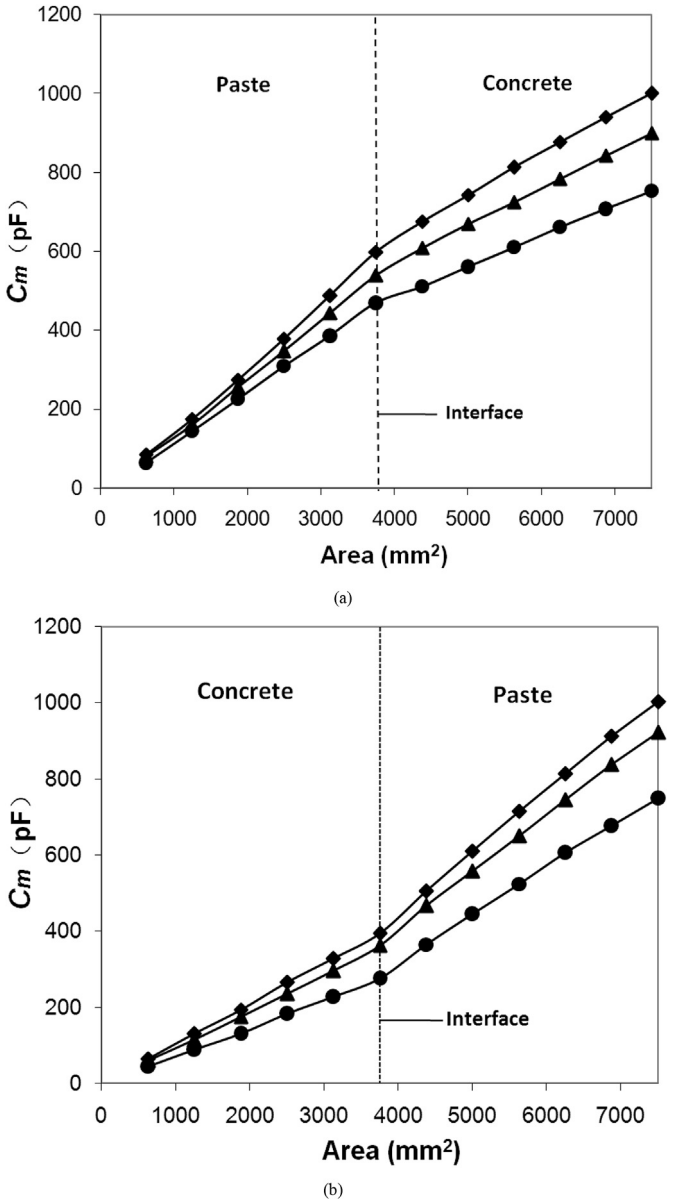

Fig. 11. The plot of the measured capacitance C_m vs. electrode area (NA) corresponding to $N = 1, 2, \ldots, 12$ and involving configuration B. The vertical dashed line indicates the location of the interface between the two regions, which are cement paste and concrete. ◆ $g = 15$ mm, ▲ $g = 30$ mm, ● $g = 70$ mm. (a) The increase in N is in the direction from cement paste to concrete. (b) The increase in N is in the direction from concrete to cement paste.

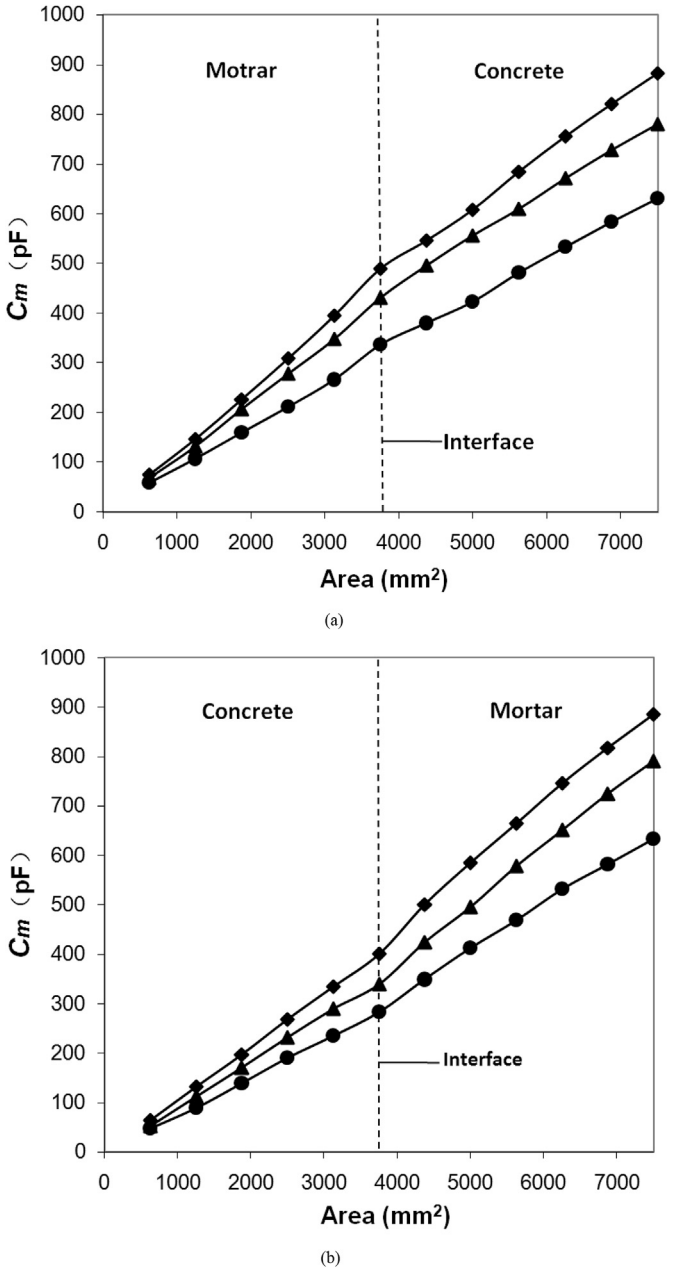

Fig. 12. The plot of the measured capacitance C_m vs. electrode area (NA) corresponding to $N = 1, 2, \ldots, 12$ and involving configuration B. The vertical dashed line indicates the location of the interface between the two regions, which are mortar and concrete. ◆ $g = 15$ mm, ▲ $g = 30$ mm, ● $g = 70$ mm. (a) The increase in N is in the direction from mortar to concrete. (b) The increase in N is in the direction from concrete to mortar.

lower value of g is recommended.

For both configurations A and B, the change in slope occurs at the interface between the two regions. Thus, the change in slope serves as an indicator of the aggregate proportion change in the NDE. In addition, the degree of linearity of the curve in a region provides an indication of the degree of uniformity of the aggregate proportion in the region. In this work, the aggregate proportion is uniform in each region, so the curve is linear within each region.

4. Methodology discussion

In this work, the interface between two regions is straight geometrically. However, it does not have to be straight, as the measurement is conducted along a line that intersects a particular point along this interface.

In this work, the series of electrodes is in a direction that is perpendicular to the interface between regions of different aggregate proportions. Though the perpendicular configuration is preferred, it is not required.

The series of squares that constitute an electrode does not need to include a square that extends across or touches the interface of the two regions. This is because the linear curve on each side of the interface can be established with three or more data points away from the interface and the intersection of the linear curves of the two sides provides indication of the position of the interface.

By decreasing the size of each square in the electrode series, the

Table 2
Slope of the curve of the measured capacitance C_m vs. electrode area, obtained using configuration B. The apparent permittivity cannot be obtained using configuration B, because the cross-sectional area of the current path is not well defined. g = distance between the proximate edges of the two electrodes.

Direction of increasing N	Slope (pF/mm^2)								
	Cement paste			Mortar			Concrete		
g (mm)	15	30	70	15	30	70	15	30	70
From paste to mortar	0.161 ± 0.010	0.148 ± 0.017	0.124 ± 0.009	0.128 ± 0.008	0.112 ± 0.011	0.086 ± 0.006	/	/	/
From mortar to paste	0.158 ± 0.009	0.148 ± 0.006	0.125 ± 0.008	0.122 ± 0.008	0.113 ± 0.007	0.086 ± 0.005	/	/	/
From mortar to concrete	/	/	/	0.133 ± 0.011	0.116 ± 0.010	0.089 ± 0.014	0.105 ± 0.011	0.091 ± 0.007	0.078 ± 0.007
From concrete to mortar	/	/	/	0.129 ± 0.010	0.117 ± 0.011	0.093 ± 0.009	0.107 ± 0.005	0.092 ± 0.007	0.075 ± 0.005
From paste to concrete	0.164 ± 0.008	0.146 ± 0.004	0.130 ± 0.005	/	/	/	0.108 ± 0.008	0.096 ± 0.003	0.076 ± 0.005
From concrete to paste	0.162 ± 0.009	0.149 ± 0.006	0.126 ± 0.008	/	/	/	0.106 ± 0.007	0.097 ± 0.005	0.074 ± 0.007

error in the determination of the location of the interface between regions with different aggregate proportions is expected to be reduced. By increasing the size of the slab, the error would also be reduced. Since the size of a structural slab is much larger than the size used in this work, the error in practical implementation will be small even using the same square size (25 mm) as this work.

In practical implementation, configuration B is more convenient than configuration A. This is because configuration A requires the presence of electrodes on two opposite surfaces, whereas configuration B requires electrodes on the same surface. The convenience associated with configuration B is particularly great in case that the cement-based structure is large or has non-parallel surfaces. On the other hand, configuration A is advantageous for detecting the internal flaws, particularly when the thickness is large, since the electric field goes through the entire thickness of the material. In contrast, configuration B only detects flaws that are in the surface region, with this limitation being particularly significant when the thickness is large. In general, configurations A and B may be used in a complementary manner for various parts of the same structure.

5. Analysis of the paste volume fraction and its impact on the permittivity

Based on the Rule of Mixtures and the masses and densities of the constituents (Sec. 2.1), the volume fractions of paste and sand in the mortar are calculated to be 0.432 and 0.568, respectively, and the volume fractions of paste, sand and gravel in the concrete are calculated to be 0.373, 0.241 and 0.386, respectively. Hence, the volume fraction of paste is higher in the mortar (0.432) than the concrete (0.373), as expected. Obviously, the volume fraction is paste is 1.000 for the cement paste. Thus, the paste volume fraction is much higher in cement paste than either mortar or concrete and the difference in the paste volume fraction between the mortar and concrete is relatively small.

The relative permittivity of cement paste with silica fume at 28 days of curing is 28 at 2 kHz [12]. The relative permittivity of sand and gravel is 2.0 and 2.6, respectively [13]. Based on the Rule of Mixtures for constituents in parallel electrically and the above-mentioned volume fractions of the constituents, the true relative permittivity is calculated to be 28, 13.2 and 11.9 for the cement paste, mortar and concrete, respectively. Hence, the ratio of the true permittivity of cement paste to mortar to concrete is 28: 13.2: 11.9 = 2.35: 1.11: 1.00. Based on Table 1, the ratio of the apparent permittivity of cement paste to mortar to concrete is 310: 230: 205 = 1.51: 1.12: 1.00. Comparison of the true permittivity ratio to the apparent permittivity ratio shows that the ratio for mortar to concrete is essentially the same for the true relative permittivity (1.11) and apparent relative permittivity (1.12), but the ratio for cement paste to concrete is considerably lower for the apparent permittivity (1.51) than the true permittivity (2.35). This difference between apparent and true permittivity in relation to the ratio of paste to concrete is attributed to the high value of the apparent permittivity of concrete (205), compared to the low value of the true permittivity of concrete (11.9).

The above analysis shows that the paste volume fraction correlates roughly with the apparent permittivity measured in this work. The paste volume fraction decreases in the order from paste to mortar and to concrete, while the permittivity decreases in the same order.

6. Difference from prior work

This paper differs from prior work in both the method and purpose. This paper involves measuring the capacitance and permittivity for probing the aggregate proportion in cement-based materials. Prior work on cement-based materials has not used electrical measurement for probing the aggregate proportion, but has involved various types of electrical measurement for probing aspects of the structure or state of cement-based materials. For example, capacitance and permittivity measurement has been used to probe the defects [4] and latex [14] in cement-based materials. Electrical polarization in cement-based materials has been studied by electrical resistance measurement [15,16]. Electrical resistance measurement has been used to probe the strain [17–23], stress [24], defects [25] and damage [26–31] in cement-based materials. Electrical conductivity measurement has been used to probe the distribution and morphology of the carbon fillers in cement-based materials [32–35], in addition to studying the shrinkage during hydration [7]. Electric current measurement has been used to probe the chloride ion permeability of cement-based materials [36]. Resistance heating has been used for providing self-heating cement-based materials [37,38].

Although electromagnetic interference shielding in the radio wave regime relates to the permittivity and this behavior has been reported in cement-based materials [39–41], the frequency range is far from that of the permittivity study of this paper. The piezoelectret behavior also relates to the permittivity and has been reported in cement-based materials [42,43], but this electromechanical behavior differs from the purely electrical behavior addressed in this paper. The thermoelectric behavior previously reported for cement-based materials [44–50] also differs from the purely electrical behavior addressed in this paper.

7. Conclusion

This paper provides the first report of capacitance-based nondestructive detection of aggregate proportion variation (i.e., cement paste proportion variation) in a cement-based material. It is based on the use of the fringing electric field (2 kHz) of a capacitor that comprises a cement-based slab (300 × 150 × 19.5 mm^3) and two copper electrodes that are separated from the slab by an electrically insulating (dielectric) film held by adhesion and that is

much smaller in area than the slab. The film is used because an RLC meter is not designed for measuring the capacitance of a conductive material. (The necessity of the film depends on the conductivity of the particular cement-based material.)

Due to the strong fringing field emanating from the electrodes and going through the slab, the apparent permittivity is high (310, 230 and 205 for cement paste, mortar and concrete, respectively). The high apparent permittivity results in high measured capacitance, which is thus sensitive to the aggregate proportion in the slab. The aggregate proportion inversely relates to the paste volume fraction, which decreases from cement paste to mortar and to concrete, thus causing the apparent permittivity to decrease in the same order.

Each slab consists of two halves (150×150 mm^2 each) that are made of cement-based materials with two different aggregate proportions. Three aggregate proportions used correspond to cement paste, mortar and concrete.

The through-thickness capacitance, which relates to the apparent relative permittivity of the cement-based material, is measured using electrodes that sandwich the slab (configuration A). In contrast, the in-plane capacitance is measured using closely spaced parallel electrodes on the same surface of the slab (configuration B).

To determine the position of the interface of the two regions with different aggregate proportions, the capacitance is measured using a series of electrodes, with each electrode geometry consisting of N squares (25×25 mm^2 for each square) linearly aligned perpendicular to the interface. The capacitance is measured in order of increasing N, which is sufficient for the electrode to cover regions on the two sides of the interface. The capacitance increases linearly with N in each region, with the slope being different for the two regions, due to the difference in the apparent permittivity. The slope (which excludes the influence of the capacitance associated with the electrodes) rather than the capacitance value (which includes the influence of the electrodes) is used as the indicator. The intersection of the extrapolated linear curves of the two regions gives the position of the interface.

The in-plane capacitance increases with decreasing spacing between the electrodes. With spacing 15 mm, the capacitance per unit electrode area is 0.16, 0.13 and 0.11 pF/mm^2 for cement paste, mortar and concrete, respectively. This trend is consistent with that of the apparent permittivity.

Acknowledgement

The authors thank the Education Department of Fujian Province and Wuyi University for financial support of the first author (Wang).

References

[1] Wen S, Chung DDL. Cement-based materials for stress sensing by dielectric measurement. Cem Concr Res 2002;32(9):1429–33.
[2] Wen S, Chung DDL. Effect of admixtures on the dielectric constant of cement paste. Cem Concr Res 2001;31(4):673–7.
[3] Wang Y, Chung DDL. Effect of the fringing electric field on the apparent electric permittivity of cement-based materials. Compos part b 2017;126:192–201.
[4] Wang Y, Chung DDL. Capacitance-based defect detection and defect location determination for cement-based material. Mater. Struct 2017 (in press).
[5] http://www.aso-cement.jp/en/products/product_ordinary.html (as viewed on May 23, 2017).
[6] http://www.lafarge-na.com/MSDS_North_America_English_-_Portland_Cement.pdf (as viewed on May 23, 2017).
[7] Cao J, Chung DDL. Microstructural effect of the shrinkage of cement-based materials during hydration, as indicated by electrical resistivity measurement. Cem Concr Res 2004;34(10):1893–7.
[8] Xu Y, Chung DDL. Improving silica fume cement by using silane. Cem Concr Res 2000;30(8):1305–11.
[9] Xu Y, Chung DDL. Cement-based materials improved by surface treated admixtures. ACI Mater J 2000;97(3):333–42.
[10] Xu Y, Chung DDL. Improving silica fume cement by using silane. Cem Concr Res 2000;30(8):305–1311.
[11] Wang S, Chung DDL. Dielectric and electrical conduction behavior of carbon paste electrochemical electrodes, with decoupling of carbon, electrolyte and interface contributions. Carbon 2014;72:135–51.
[12] Haddad AS, Chung DDL. Decreasing the electric permittivity of cement by graphite particle incorporation. Carbon 2017;122C:702–9.
[13] https://www.vega.com/home_ss/-/media/PDF-files/List_of_dielectric_constants_EN.ashx (as viewed on June 7, 2017).
[14] Wang M, Chung DDL. Understanding the increase of the electric permittivity of cement caused by latex addition. Composites part b, submitted.
[15] Cao J, Chung DDL. Electric polarization and depolarization in cement-based materials, studied by apparent electrical resistance measurement. Cem Concr Res 2004;34(3):481–5.
[16] Wen S, Chung DDL. Electric polarization in carbon fiber reinforced cement. Cem Concr Res 2001;31(2):141–7.
[17] Chung DDL. Cement reinforced with short carbon fibers: a multifunctional material. Compos part b 2000;31(6–7):511–26.
[18] Wen S, Chung DDL. Piezoresistivity-based strain sensing in carbon fiber reinforced cement. ACI Mater J 2007;104(2):171–9.
[19] Zhu S, Chung DDL. Theory of piezoresistivity for strain sensing in carbon fiber reinforced cement under flexure. J Mater Sci 2007;42(15):6222–33.
[20] Wen S, Chung DDL. Effects of strain and damage on the strain sensing ability of carbon fiber cement. J Mater Civ Eng 2006;18(3):355–60.
[21] Wen S, Chung DDL. Spatially resolved self-sensing of strain and damage in carbon fiber cement. J Mater Sci 2006;41(15):4823–31.
[22] Chen P, Chung DDL. Concrete as a new strain/stress sensor. Compos part b 1996;27(1):11–23.
[23] Wen S, Chung DDL. Strain sensing characteristics of carbon fiber reinforced cement. ACI Mater J 2005;102(4):244–8.
[24] Hoheneder J, Flores-Vivian I, Lin Z, Zilberman P, Sobolev K. Performance of stress-sensing smart fiber reinforced composites in moist and sodium chloride environments. Compos part b 2015;73:89–95.
[25] Cao J, Wen S, Chung DDL. Defect dynamics and damage of cement-based materials, studied by electrical resistance measurement. J Mater Sci 2001;36(18):4351–60.
[26] Wen S, Chung DDL. Electrical-resistance-based damage self-sensing in carbon fiber reinforced cement. Carbon 2007;45(4):710–6.
[27] Wen S, Chung DDL. Self-sensing of flexural damage and strain in carbon fiber reinforced cement and effect of embedded steel reinforcing bars. Carbon 2006;44(8):1496–502.
[28] Meehan DG, Wang S, Chung DDL. Electrical-resistance-based sensing of impact damage in carbon fiber reinforced cement-based materials. J Intell Mater Syst Struct 2010;21(1):83–105.
[29] Cao J, Chung DDL. Damage evolution during freeze-thaw cycling of cement mortar, studied by electrical resistivity measurement. Cem Concr Res 2002;32(10):1657–61.
[30] Cao J, Chung DDL. Degradation of the bond between old and new mortar under cyclic shear loading, monitored by contact electrical resistance measurement. Cem Concr Res 2001;31(11):1647–51.
[31] Cao J, Chung DDL. Minor damage of cement mortar during cyclic compression, monitored by electrical resistivity measurement. Cem Concr Res 2001;31(10):1519–21.
[32] Xie N, Shi X, Feng D, Kuang B, Li H. Percolation backbone structure analysis in electrically conductive carbon fiber reinforced cement composites. Compos part b 2012;43(8):3270–5.
[33] García-Macías E, D'Alessandro A, Castro-Triguero R, Pérez-Mira D, Ubertini F. Micromechanics modeling of the electrical conductivity of carbon nanotube cement-matrix composites. Compos part b 2017;108:451–69.
[34] Wen S, Chung DDL. Double percolation in the electrical conduction in carbon fiber reinforced cement-based materials. Carbon 2007;45(2):263–7.
[35] Baeza FJ, Chung DDL, Zornoza E, Andión LG, Garcés P. Triple percolation in concrete reinforced with carbon fiber. ACI Mater J 2010;107(4):396–402.
[36] Güneyisi E, Özturan T, Gesoğlu M. Examining the electrical properties of plain and blended cement concretes: relationship between charge passed and initial current. Compos part b 2011;42(6):1517–24.
[37] Wang S, Wen S, Chung DDL. Resistance heating using electrically conductive cements. Adv Cem Res 2004;16(4):161–6.
[38] Hambach M, Möller H, Neumann T, Volkmer D. Carbon fibre reinforced cement-based composites as smart floor heating materials. Compos part b 2016;90:465–70.
[39] Muthusamy S, Chung DDL. Carbon fiber cement-based materials for electromagnetic interference shielding. ACI Mater J 2010;107(6):602–10.
[40] Cao J, Chung DDL. Use of fly ash as an admixture for electromagnetic interference shielding. Cem Concr Res 2004;34(10):1889–92.
[41] Wen S, Chung DDL. Electromagnetic interference shielding reaching 70 dB in steel fiber cement. Cem Concr Res 2004;34(2):329–32.
[42] Huang C, Wang S, Chung DDL. Cement-based piezoelectret. Mater Struct 2009;42:541–57.
[43] Huang C, Chung DDL. Controlling and increasing the inherent voltage in cement paste. Adv Cem Res 2009;21(1):31–7.
[44] Wen S, Chung DDL. Thermoelectric behavior of carbon-cement composites. Carbon 2002;40(13):2495–7.

[45] Wen S, Chung DDL. Origin of the thermoelectric behavior of steel fiber cement paste. Cem Concr Res 2002;32(5):821–3.
[46] Wen S, Chung DDL. Effect of fiber content on the thermoelectric behavior of cement. J Mater Sci 2004;39(13):4103–6.
[47] Wen S, Chung DDL. Cement as a thermoelectric material. J Mater Res 2000;15(12):2844–8.
[48] Wen S, Chung DDL. Erratum: cement as a thermoelectric material. J Mater Res 2004;19(4):1294.
[49] Wen S, Chung DDL. Rectifying and thermocouple junctions based on Portland cement. J Mater Res 2001;16(7):1989–93.
[50] Wen S, Chung DDL. Erratum: rectifying and thermocouple junctions based on Portland cement. J Mater Res 2004;19(4):1294.